Science Advances
AAAS

advances.sciencemag.org/cgi/content/full/7/28/eabf6222/DC1

Supplementary Materials for

Survival of presolar *p*-nuclide carriers in the nebula revealed by stepwise leaching of Allende refractory inclusions

Bruce L. A. Charlier*, François L. H. Tissot, Hauke Vollstaedt, Nicolas Dauphas, Colin J. N. Wilson, Ren T. Marquez

*Corresponding author. Email: bruce.charlier@vuw.ac.nz

Published 9 July 2021, *Sci. Adv.* **7**, eabf6222 (2021)
DOI: 10.1126/sciadv.abf6222

This PDF file includes:

Figs. S1 to S14
Tables S1 to S6
References

Supplementary Materials

CAI specimen *Charles*

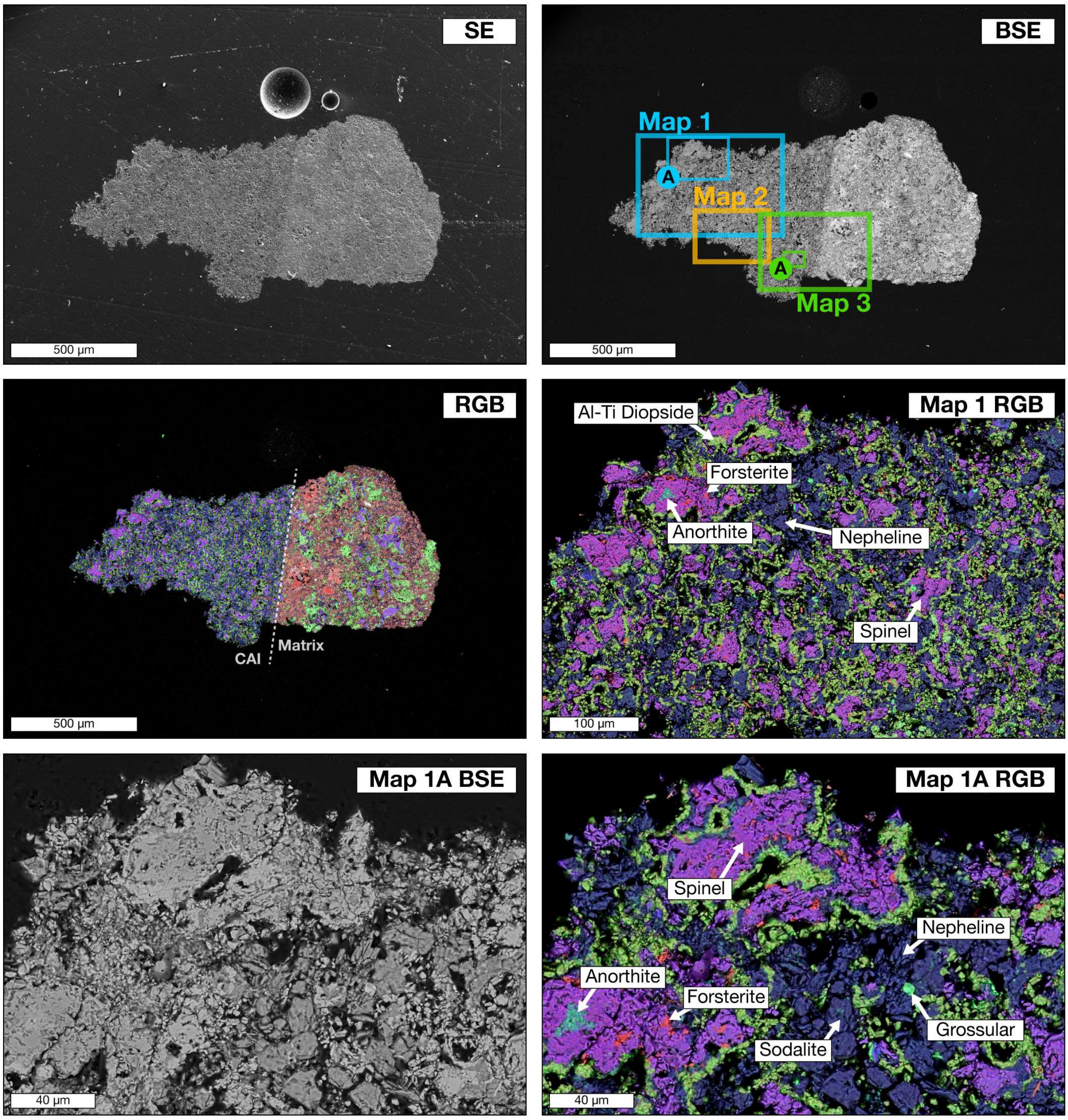

Fig. S1. Secondary Electron (SE) and Back Scattered Electron (BSE) images with false color RGB (Mg/Ca/Al) maps of selected fields of view identified as representative of the specimen. Marked areas denote maps (identified by map number) made for certain parts of the CAI. Sub-maps are delineated using the same color and identified with sub-map letters (*i.e.*, sub-map 1A for area A within map 1). Note the different scales on different maps and sub-maps.

CAI specimen *Erik*

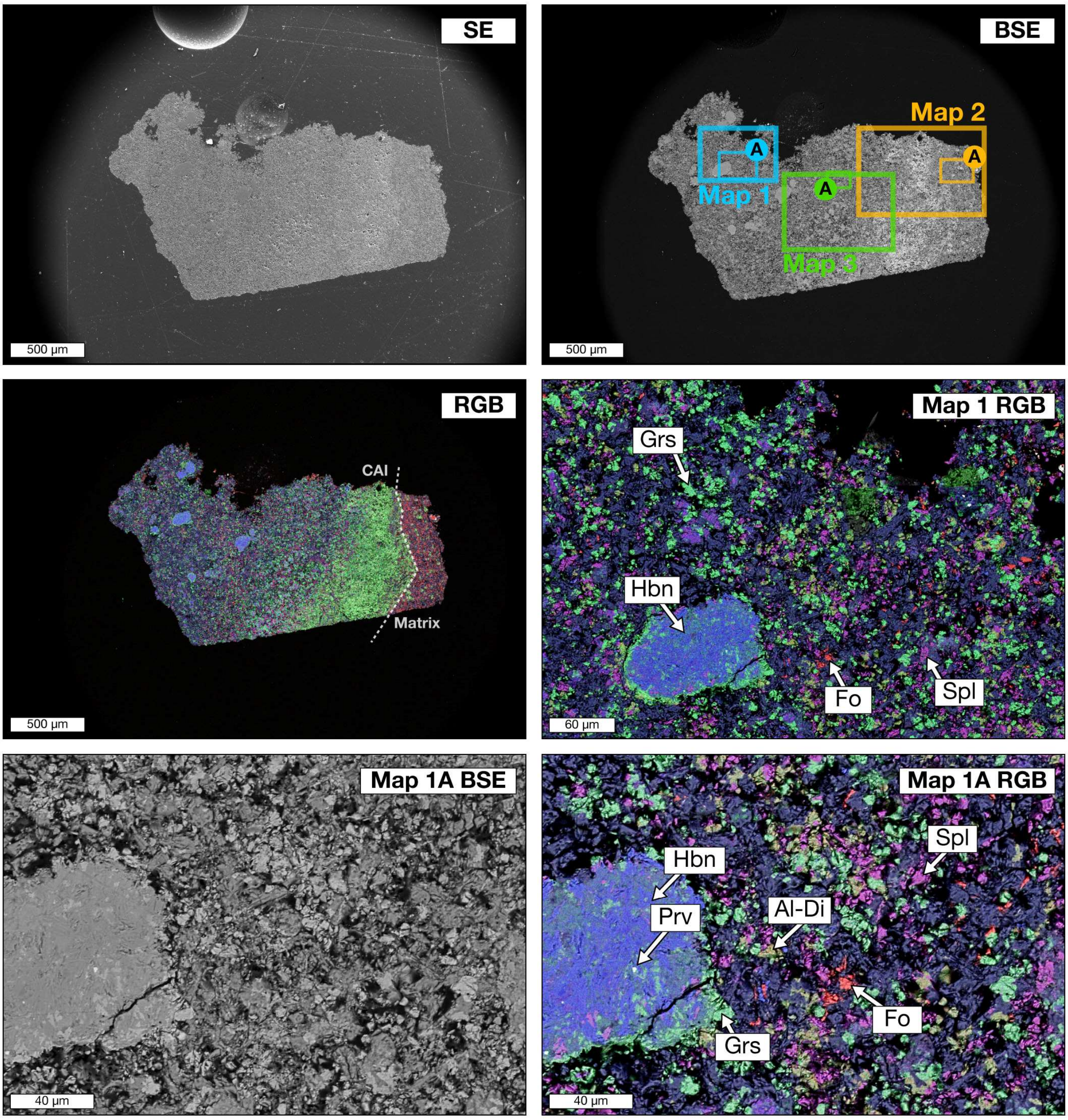

Fig. S2. Secondary Electron (SE) and Back Scattered Electron (BSE) images with false color RGB (Mg/Ca/Al) maps of selected fields of view identified as representative of the specimen. Marked areas denote maps (identified by map number) made for certain parts of the CAI. Sub-maps are delineated using the same color and identified with sub-map letters (*i.e.*, sub-map 1A for area A within map 1). Note the different scales on different maps and sub-maps.

CAI specimen *Hank*

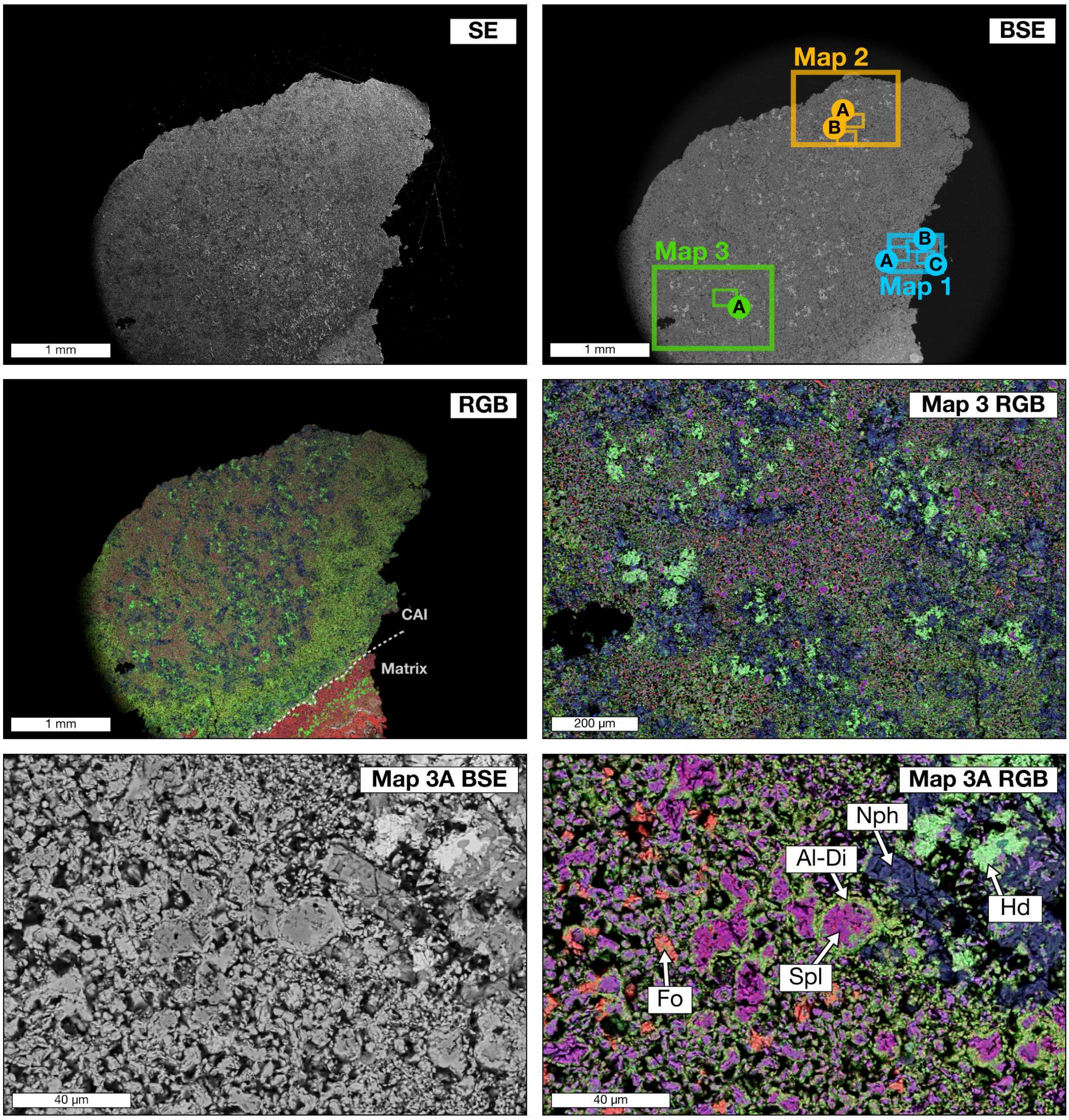

Fig. S3. Secondary Electron (SE) and Back Scattered Electron (BSE) images with false color RGB (Mg/Ca/Al) maps of selected fields of view identified as representative of the specimen. Marked areas denote maps (identified by map number) made for certain parts of the CAI. Sub-maps are delineated using the same color and identified with sub-map letters (*i.e.*, sub-map 1A for area A within map 1). Note the different scales on different maps and sub-maps.

CAI specimen *Jean*

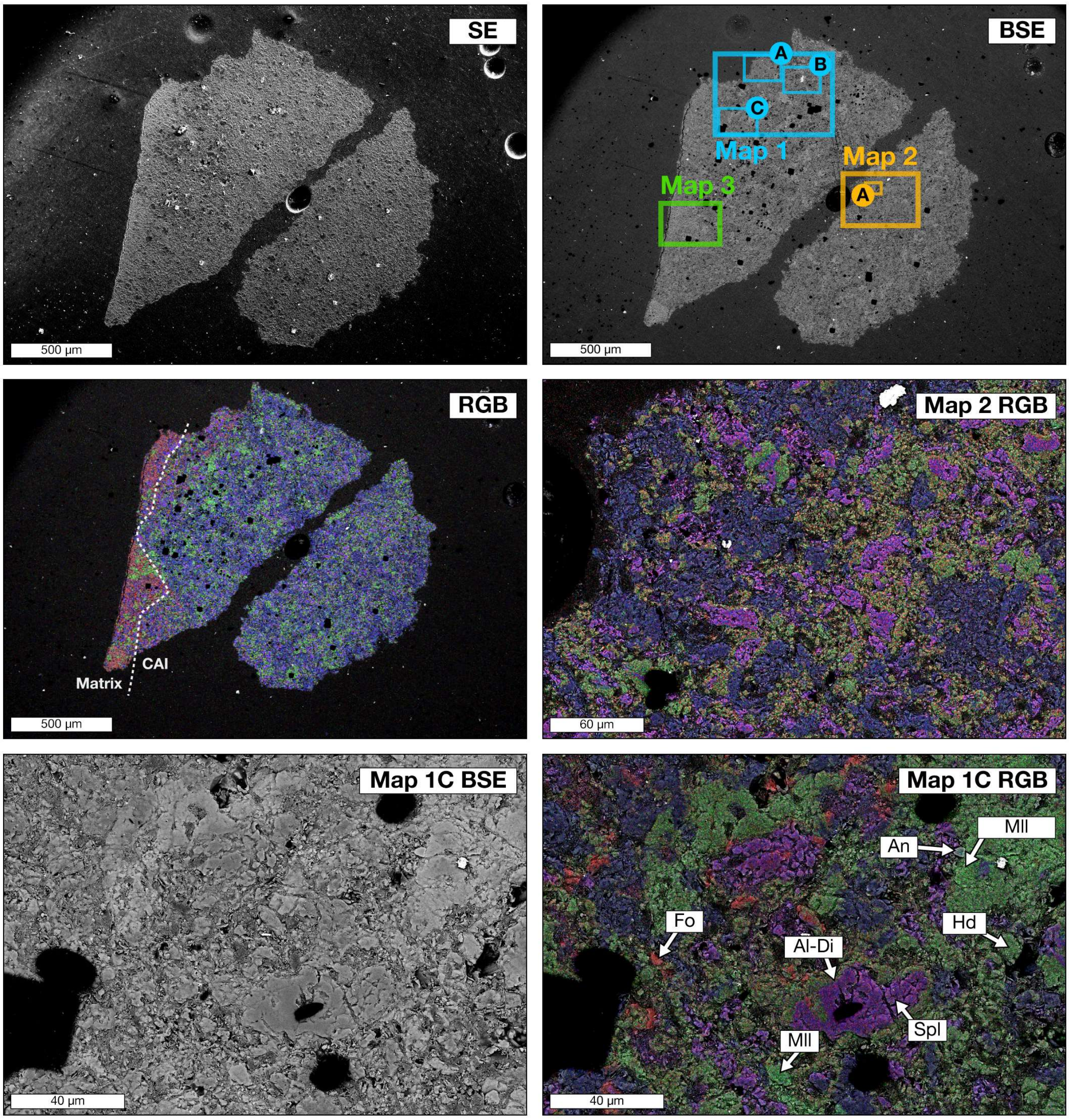

Fig. S4. Secondary Electron (SE) and Back Scattered Electron (BSE) images with false color RGB (Mg/Ca/Al) maps of selected fields of view identified as representative of the specimen. Marked areas denote maps (identified by map number) made for certain parts of the CAI. Sub-maps are delineated using the same color and identified with sub-map letters (*i.e.*, sub-map 1A for area A within map 1). Note the different scales on different maps and sub-maps.

CAI specimen *Logan*

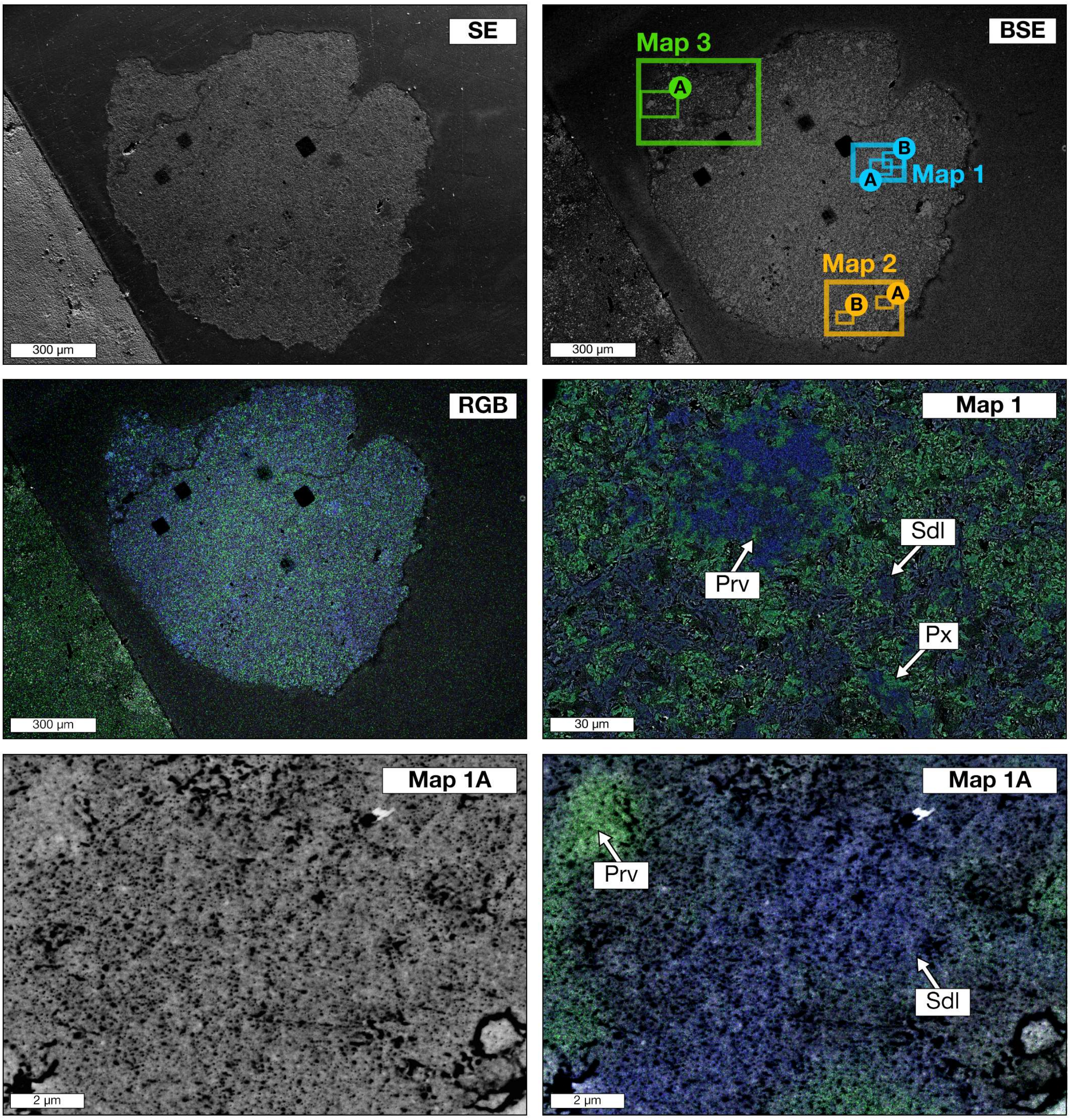

Fig. S5. Secondary Electron (SE) and Back Scattered Electron (BSE) images with false color RGB (Mg/Ca/Al) maps of selected fields of view identified as representative of the specimen. Marked areas denote maps (identified by map number) made for certain parts of the CAI. Sub-maps are delineated using the same color and identified with sub-map letters (*i.e.*, sub-map 1A for area A within map 1). Note the different scales on different maps and sub-maps.

CAI specimen *Ororo*

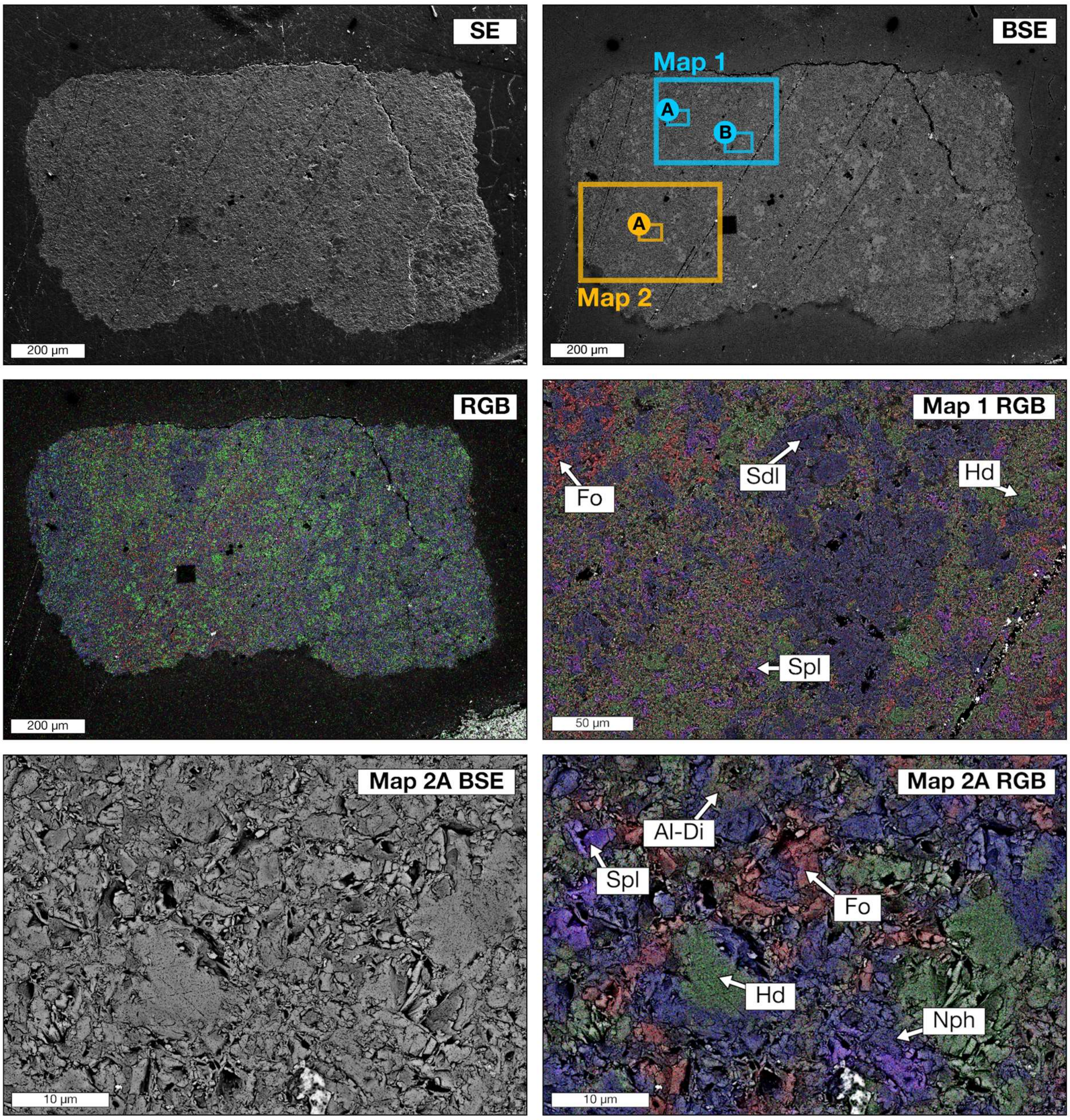

Fig. S6. Secondary Electron (SE) and Back Scattered Electron (BSE) images with false color RGB (Mg/Ca/Al) maps of selected fields of view identified as representative of the specimen. Marked areas denote maps (identified by map number) made for certain parts of the CAI. Sub-maps are delineated using the same color and identified with sub-map letters (*i.e.*, sub-map 1A for area A within map 1). Note the different scales on different maps and sub-maps.

CAI specimen *Peter*

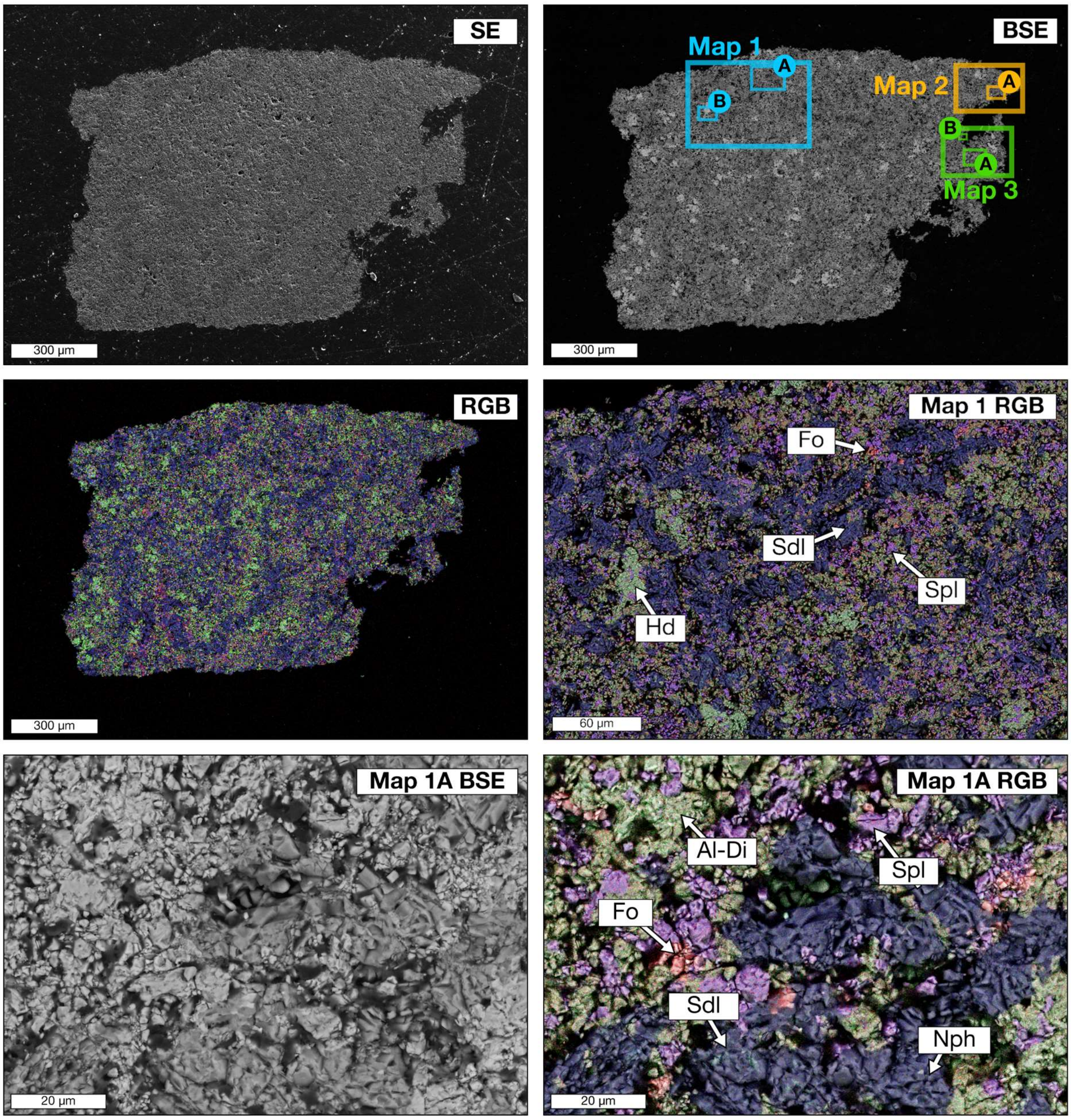

Fig. S7. Secondary Electron (SE) and Back Scattered Electron (BSE) images with false color RGB (Mg/Ca/Al) maps of selected fields of view identified as representative of the specimen. Marked areas denote maps (identified by map number) made for certain parts of the CAI. Sub-maps are delineated using the same color and identified with sub-map letters (*i.e.*, sub-map 1A for area A within map 1). Note the different scales on different maps and sub-maps.

CAI specimen *Raven*

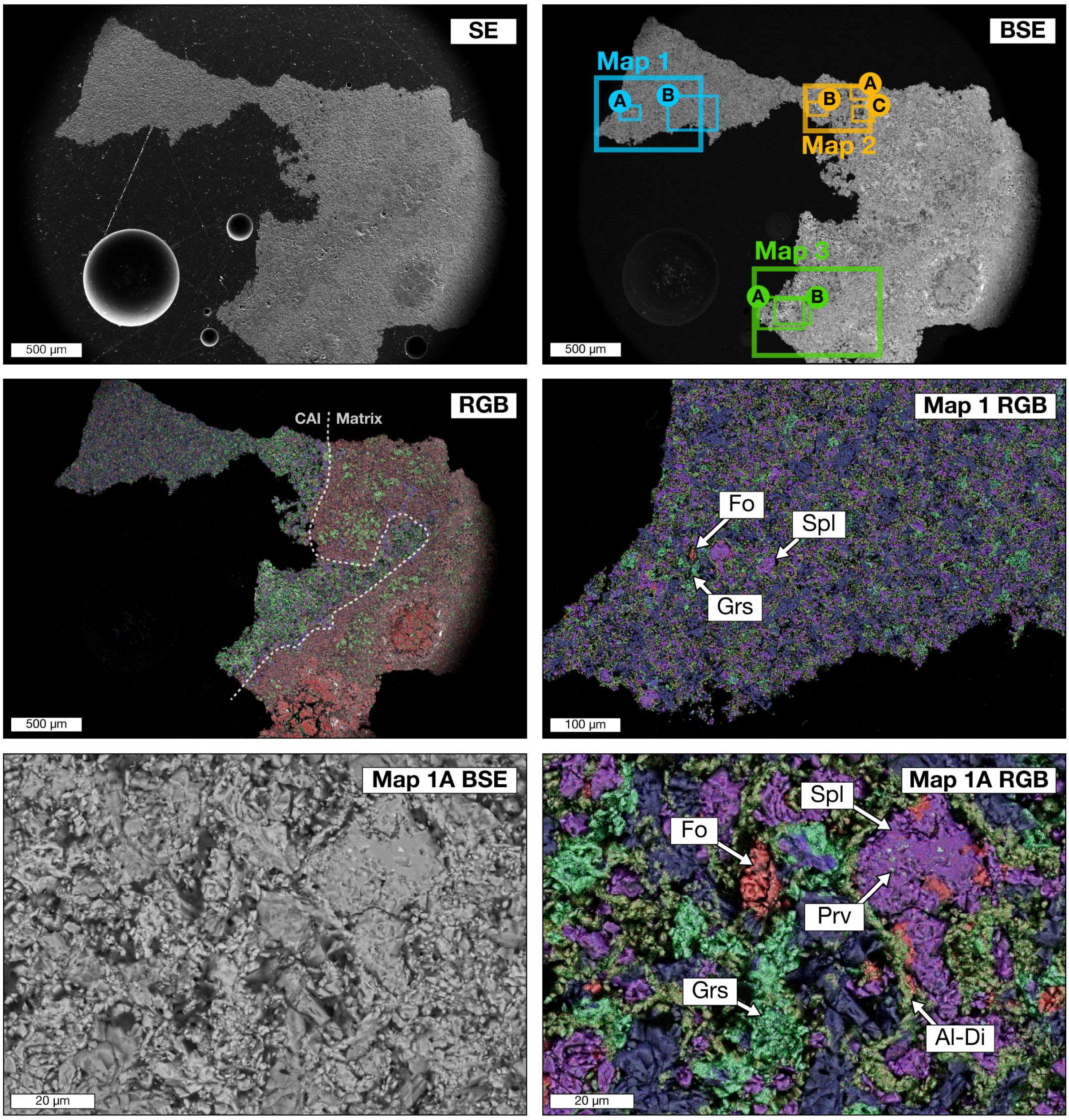

Fig. S8. Secondary Electron (SE) and Back Scattered Electron (BSE) images with false color RGB (Mg/Ca/Al) maps of selected fields of view identified as representative of the specimen. Marked areas denote maps (identified by map number) made for certain parts of the CAI. Sub-maps are delineated using the same color and identified with sub-map letters (*i.e.*, sub-map 1A for area A within map 1). Note the different scales on different maps and sub-maps.

CAI specimen *Scott*

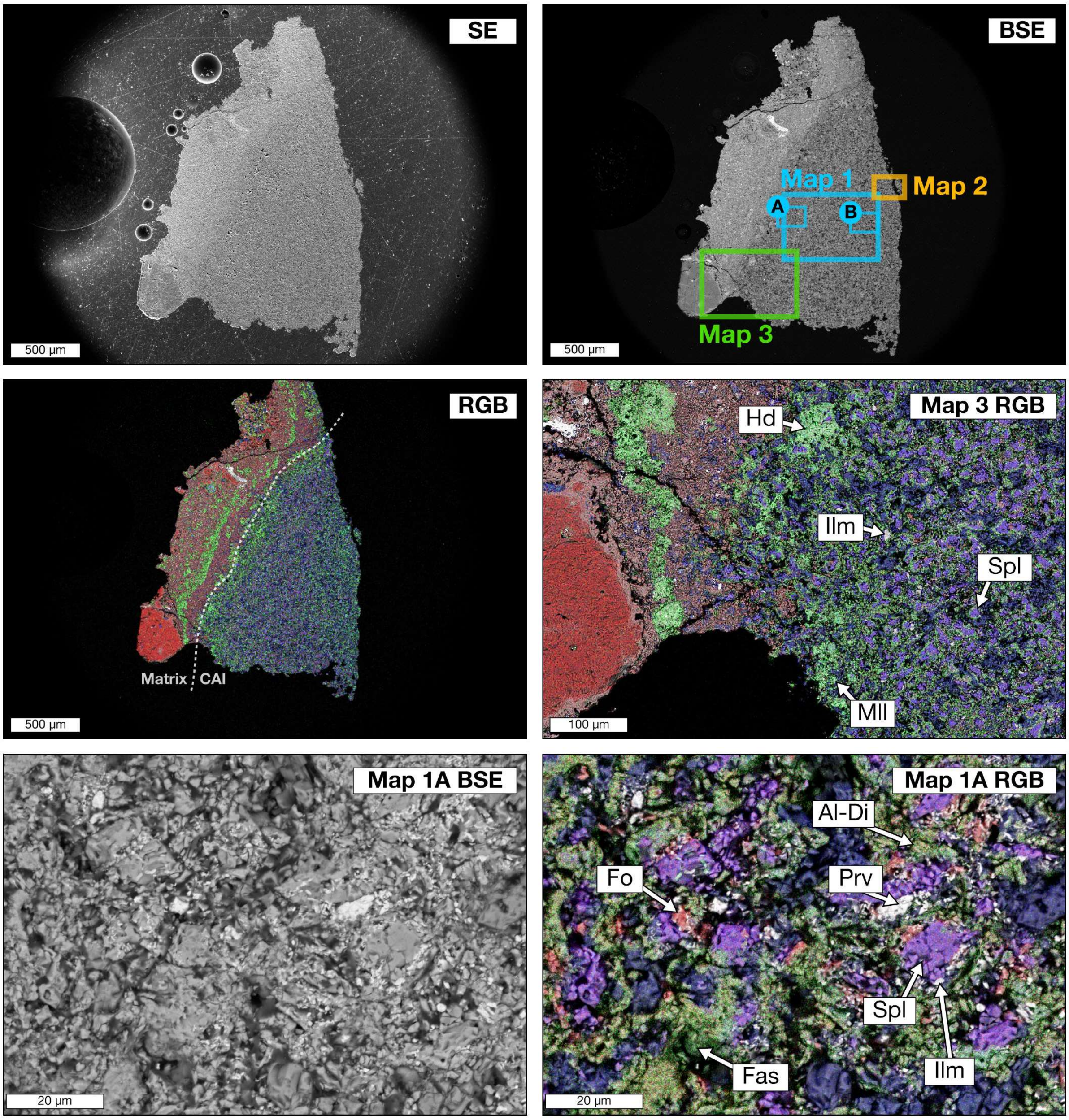

Fig. S9. Secondary Electron (SE) and Back Scattered Electron (BSE) images with false color RGB (Mg/Ca/Al) maps of selected fields of view identified as representative of the specimen. Marked areas denote maps (identified by map number) made for certain parts of the CAI. Sub-maps are delineated using the same color and identified with sub-map letters (*i.e.*, sub-map 1A for area A within map 1). Note the different scales on different maps and sub-maps.

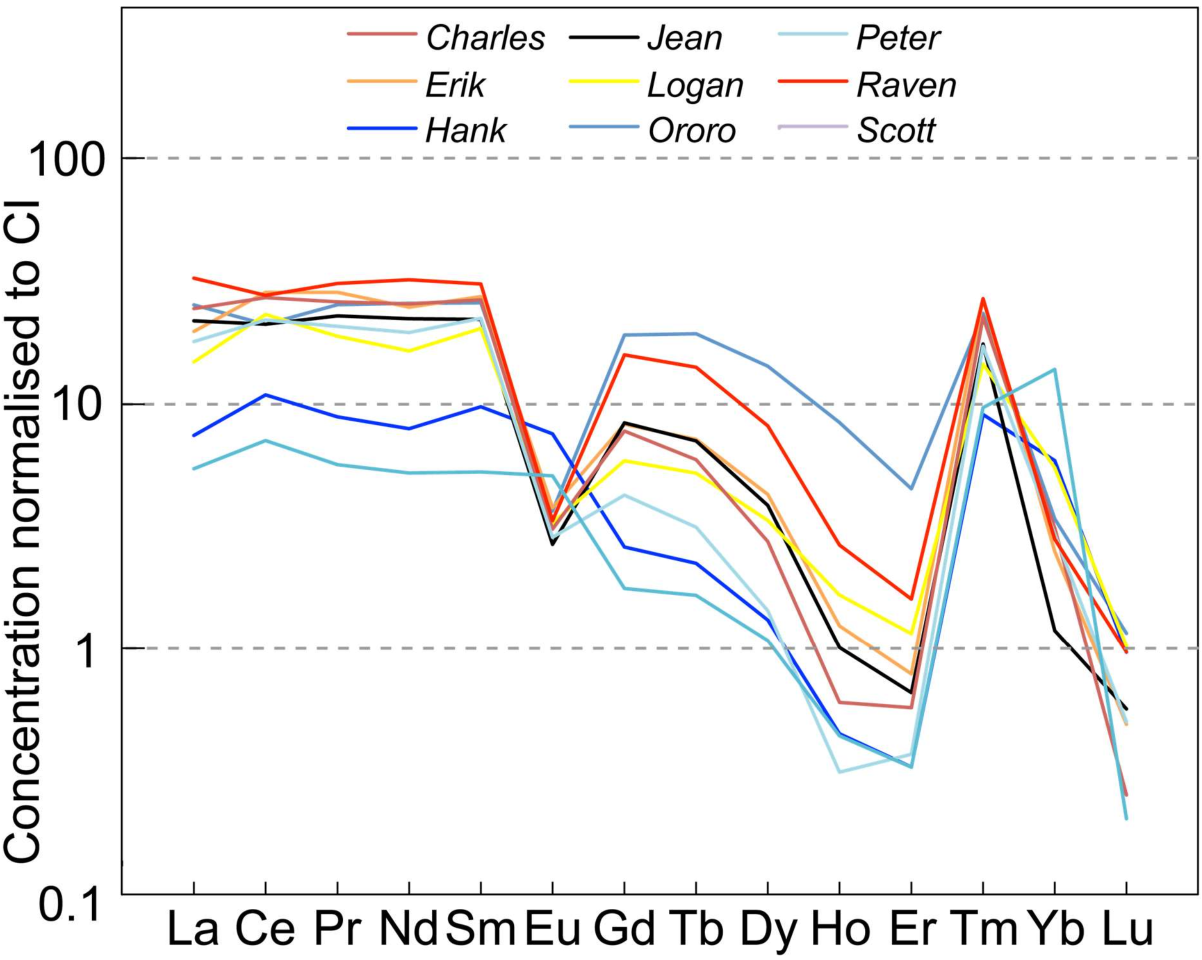

Fig. S10. REE abundance patterns for bulk digestions of the nine fine-grained CAIs used for this study (data given in Table S1). All CAIs show a group II pattern in which the most refractory (heavy REEs except Tm, Yb) and most volatile elements (Eu, Yb) are depleted relative to the moderately refractory light REEs. Values normalized to the CI chondrite values of Dauphas and Pourmand (*63*).

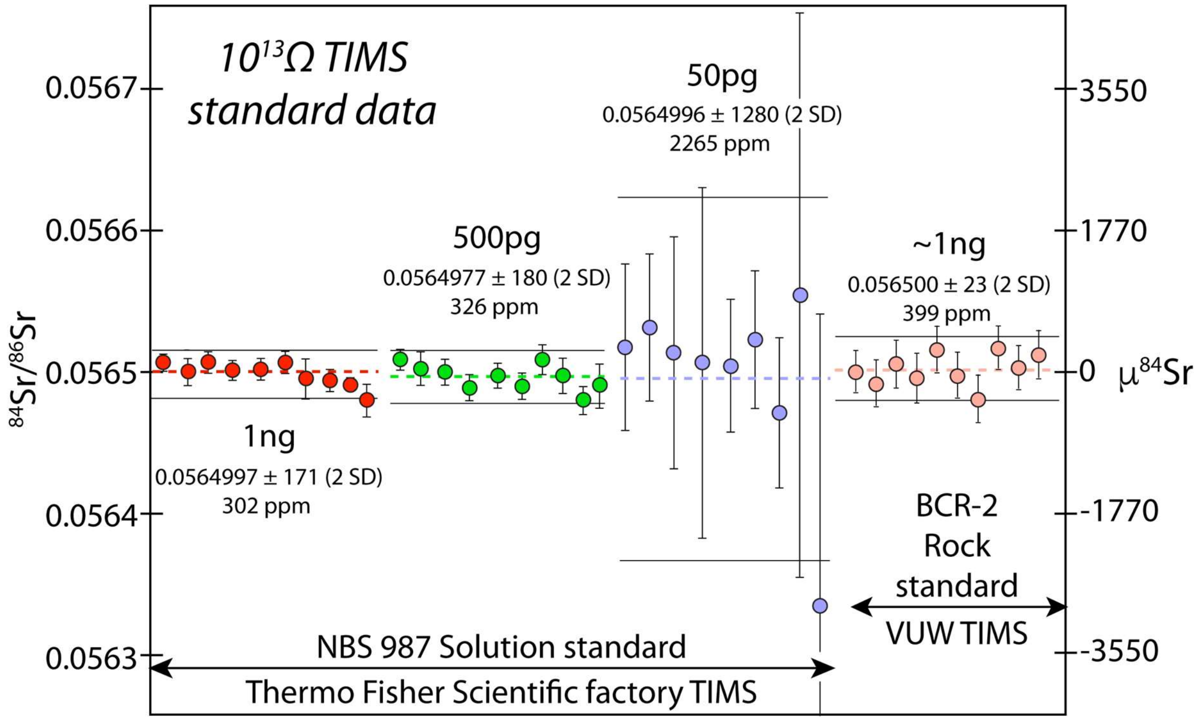

Fig. S11. Compilation of standards data for small sample loads representative of those used for unknowns in this paper. Full data are presented in Table S1 and Table S2. The data serve to demonstrate (i) that useful precision on the $^{84}Sr/^{86}Sr$ ratio ($\mu^{84}Sr$) can be obtained on loads as small as 50 pg; (ii) that column processing of the natural samples does not impose any anomalies or systematic bias; and (iii) that at no stage prior to (NBS987 data), or subsequent to, usage of the Sr double spike (BCR-2 data) is there any evidence for spike contamination (see text in supplementary material for details).

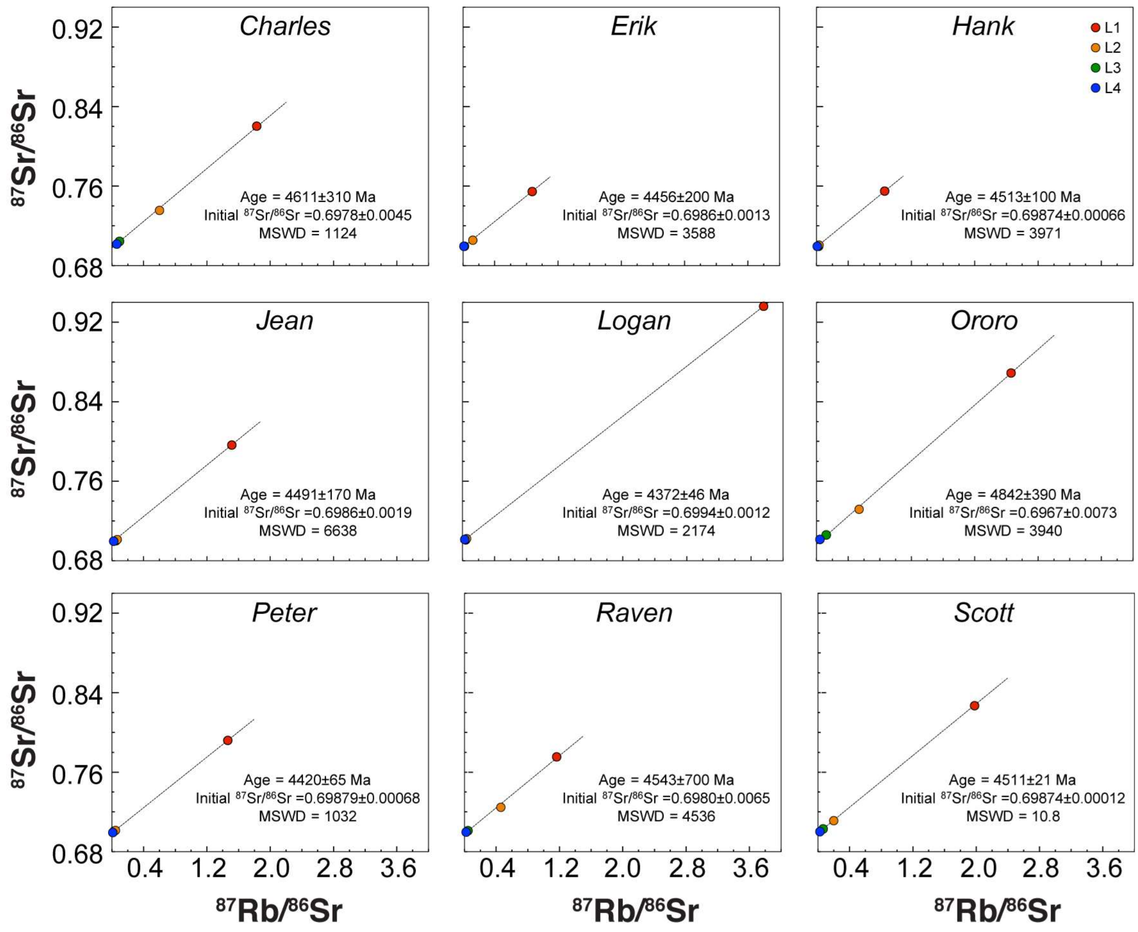

Fig. S12. ^{87}Rb-^{86}Sr isochron plots for all leach steps for individual CAIs in this study, plotted using the same scale for each panel for clarity. . The Rb-Sr regression lines used type 3 York fits implemented in Isoplot (*61*). Ages calculated using the ^{87}Rb decay constant of Rotenberg et al. (*62*).

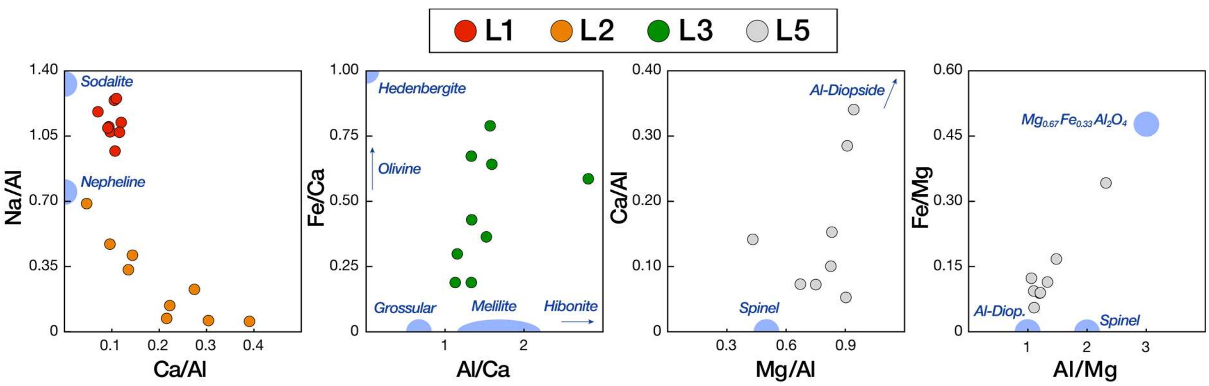

Fig. S13. Cross-plots of major element atomic ratios in solutions from individual leaching steps. Proposed end-member minerals, denoting the dominant phases getting dissolved in each step, are denoted as blue areas. From (*64*).

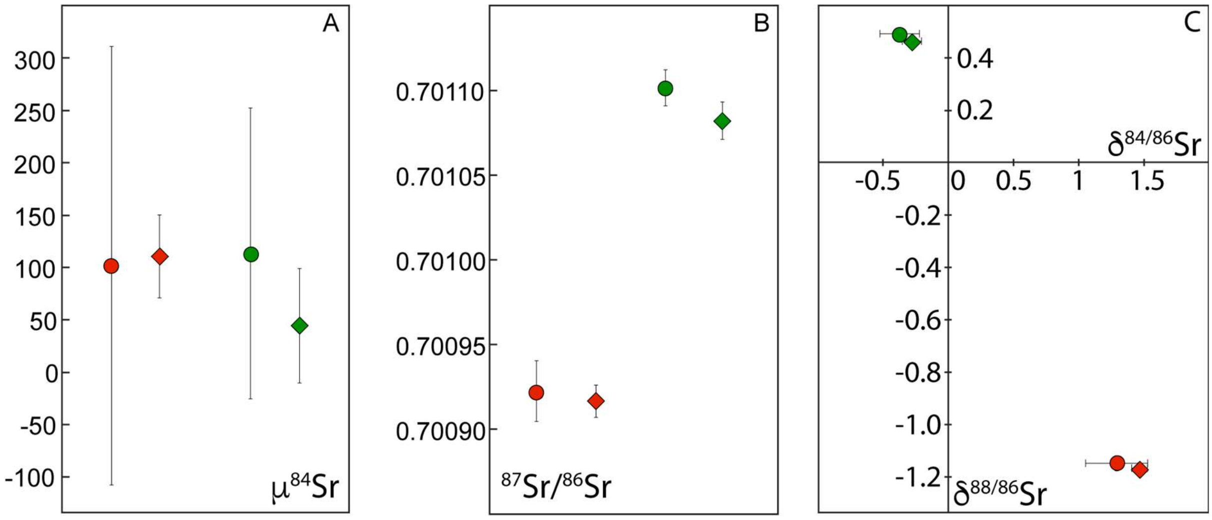

Fig. S14. Comparison data for two samples, L3_*Jean* (red symbols) and L3_*Logan* (green symbols) measured using the VUW Triton (circles) and the Thermo Scientific Triton XT (diamonds) TIMS instruments. (A) The μ^{84}Sr data were calculated relative to the average measured NBS987 ^{84}Sr/^{86}Sr for each instrument (Table S2). (B) The ^{87}Sr/^{86}Sr data were normalized to NBS987 = 0.710250 for each instrument. (C) The $\delta^{84/86}$Sr vs. $\delta^{88/86}$Sr data were calculated using the double-spiked and natural aliquots run on each instrument respectively.

Table S1. Rare earth element concentrations in bulk digests of the samples used in this study, normalized to the CI chondrite value of Dauphas and Pourmand (*63*).

	La	Ce	Pr	Nd	Sm	Eu	Gd	Tb	Dy	Ho	Er	Tm	Yb	Lu
Charles	25.3	21.1	25.4	25.7	25.8	3.7	19.1	19.3	14.3	8.4	4.5	23.4	3.4	1.2
Erik	19.7	28.5	28.5	24.8	27.4	3.8	8.3	7.2	4.3	1.3	0.8	26.7	2.5	0.5
Hank	7.5	10.9	8.9	8.0	9.8	7.6	2.6	2.3	1.3	0.5	0.3	9.1	5.9	1.0
Jean	21.8	21.1	22.8	22.2	22.1	2.7	8.4	7.1	3.9	1.0	0.7	17.5	1.2	0.6
Logan	14.8	23.1	18.9	16.5	20.3	3.3	5.9	5.2	3.4	1.7	1.2	14.6	5.5	1.0
Ororo	24.4	27.1	26.0	25.6	26.5	3.1	7.8	6.0	2.8	0.6	0.6	22.6	3.1	0.3
Peter	18.0	22.0	20.7	19.5	22.3	2.9	4.3	3.2	1.4	0.3	0.4	17.2	3.0	0.5
Raven	32.5	27.7	30.9	32.0	30.8	3.4	15.9	14.1	8.2	2.7	1.6	26.8	2.8	1.0
Scott	5.5	7.1	5.7	5.3	5.3	5.1	1.8	1.7	1.1	0.4	0.3	9.7	13.9	0.2

Table S2. NBS987 standard data for various load sizes measured using two TIMS instruments.

	$^{84}Sr/^{86}Sr$	2 s.e.	2 s.e. (ppm)	$^{87}Sr/^{86}Sr$	2 s.e.	2 s.e. (ppm)
1000 ng[1]						
Filament 1	0.0564883	0.0000009	16.2	0.710257	0.000002	3.5
Filament 2	0.0564886	0.0000010	18.1	0.710261	0.000002	3.3
Filament 3	0.0564895	0.0000010	18.2	0.710259	0.000002	3.4
Filament 4	0.0564892	0.0000010	17.0	0.710262	0.000003	3.5
Filament 5	0.0564896	0.0000010	17.8	0.710261	0.000002	3.4
Filament 6	0.0564879	0.0000010	17.7	0.710258	0.000002	3.3
Filament 7	0.0564887	0.0000010	17.6	0.710263	0.000002	3.4
Filament 8	0.0564893	0.0000010	17.3	0.710260	0.000002	3.4
Filament 9	0.0564882	0.0000009	15.7	0.710263	0.000002	3.4
Average	0.0564888			0.710260		
2 s.d.	0.0000012			0.000004		
2 s.d. (ppm)	22.0			5.9		
50 ng Sr[2]						
Filament 1	0.0564891	0.0000011	19.6	0.710260	0.000003	4.7
Filament 2	0.0564895	0.0000008	13.8	0.710262	0.000002	3.4
Filament 3	0.0564883	0.0000008	14.1	0.710260	0.000003	3.5
Filament 4	0.0564912	0.0000008	14.0	0.710254	0.000002	3.4
Filament 5	0.0564881	0.0000007	12.9	0.710255	0.000002	3.4
Filament 6	0.0564896	0.0000009	16.0	0.710261	0.000002	3.5
Filament 7	0.0564906	0.0000008	14.2	0.710257	0.000002	3.4
Filament 8	0.0564918	0.0000009	15.9	0.710260	0.000003	4.4
Filament 9	0.0564906	0.0000010	18.2	0.710262	0.000003	3.7
Filament 10	0.0564892	0.0000016	28.0	0.710261	0.000005	7.2
Average	0.0564898			0.710259		
2 s.d.	0.0000024			0.000006		
2 s.d. (ppm)	43.3			7.8		
1 ng Sr[3]						
Filament 1	0.0565080	0.0000060	107	0.710247	0.000017	25
Filament 2	0.0565013	0.0000095	169	0.710237	0.000027	38
Filament 3	0.0565081	0.0000076	135	0.710286	0.000026	36
Filament 4	0.0565025	0.0000070	124	0.710261	0.000021	30
Filament 5	0.0565033	0.0000076	135	0.710237	0.000022	31
Filament 6	0.0565082	0.0000078	138	0.710242	0.000027	39
Filament 7	0.0564965	0.0000141	250	0.710240	0.000042	59
Filament 8	0.0564954	0.0000078	139	0.710283	0.000030	43
Filament 9	0.0564927	0.0000048	84	0.710277	0.000015	21
Filament 10	0.0564812	0.0000115	204	0.710294	0.000054	77
Average	0.0564997			0.710260		
2 s.d.	0.0000171			0.000045		
2 s.d. (ppm)	302			64		
500 pg Sr[3]						
Filament 1	0.0565101	0.0000073	130	0.710269	0.000023	32
Filament 2	0.0565038	0.0000118	208	0.710253	0.000033	47
Filament 3	0.0565012	0.0000091	162	0.710247	0.000029	41
Filament 4	0.0564903	0.0000092	163	0.710251	0.000029	41
Filament 5	0.0564988	0.0000088	155	0.710246	0.000028	39
Filament 6	0.0564914	0.0000093	164	0.710227	0.000035	49
Filament 7	0.0565101	0.0000105	186	0.710226	0.000027	37
Filament 8	0.0564987	0.0000124	220	0.710246	0.000028	40
Filament 9	0.0564812	0.0000099	175	0.710294	0.000037	53
Filament 10	0.0564914	0.0000156	276	0.710225	0.000047	66
Average	0.0564977			0.710248		
2 s.d.	0.0000184			0.000043		
2 s.d. (ppm)	326			60		
50 pg Sr[3]						
Filament 1	0.0565189	0.0000587	1039	0.710300	0.000082	116
Filament 2	0.0565328	0.0000519	919	0.710159	0.000098	138
Filament 3	0.0565150	0.0000818	1448	0.710321	0.000140	197
Filament 4	0.0565078	0.0001237	2189	0.710191	0.000206	291
Filament 5	0.0565058	0.0000468	828	0.710097	0.000069	97
Filament 6	0.0565242	0.0000486	859	0.710263	0.000077	109
Filament 8	0.0564725	0.0000530	939	0.710312	0.000083	116
Filament 9	0.0565556	0.0001991	3520	0.710225	0.000327	460
Filament 10	0.0563367	0.0002056	3649	0.710235	0.000356	501
Average	0.0564966			0.710234		
2 s.d.	0.0001279			0.000150		
2 s.d. (ppm)	2265			211		

[1]Thermo-Finnigan Triton at VUW - Leaches L1 to L3

[2]Thermo-Finnigan Triton at VUW - Bulk analyses

[3]Thermo-Fisher Triton XT at Bremen factory - Leaches L4 and L5

Table S3. BCR-2 data for ~1 ng loads measured using the VUW TIMS after upgrading with 10^{13} Ω resistor amplifiers

	$^{84}Sr/^{86}Sr$	2 s.e.	2 s.e. (ppm)	$^{87}Sr/^{86}Sr$	2 s.e.	2 s.e. (ppm)
~1 ng Sr BCR-2						
	0.056498	0.000015	265	0.705020	0.000031	43
	0.056490	0.000017	293	0.705018	0.000036	51
	0.056503	0.000017	298	0.705027	0.000032	46
	0.056494	0.000018	313	0.705034	0.000034	49
	0.056514	0.000016	292	0.705035	0.000030	42
	0.056496	0.000016	286	0.705033	0.000033	46
	0.056479	0.000017	301	0.705008	0.000034	48
	0.056515	0.000015	274	0.705006	0.000032	45
	0.056501	0.000016	279	0.705053	0.000033	47
	0.056510	0.000017	302	0.705045	0.000036	51
Average	0.056500			0.705028		
2 s.d.	0.000023			0.000031		
2 s.d. (ppm)	399			43		

Table S4. Summary of strontium isotopic compositions and concentrations of step-leached CAI fractions and bulk digests.

Sample number	Instrument	Amp. Config.	Total ng Sr in aliquot[1]	Blank contrib. %[2]	$\delta^{84/86}Sr$ (‰)[3]	2 s.e.[5]	$\delta^{88/86}Sr$ (‰)[3]	2 s.e.[5]	$\mu^{84}Sr$ (ppm)	2 s.e.[5]	$^{87}Sr/^{86}Sr$[3,4]	2 s.e.[5]	2 s.e. (ppm)	Cycles	Rb (ppm)[7]	Sr (ppm)[7]	$^{87}Rb/^{86}Sr$	2 s.e.
Leach 1																		
L1_*Charles*	VUW	$10^{11}\Omega$	1030.8	0.01	1.497	0.022	-1.347	0.009	118.9	27.7	0.820328	0.000005	6.0	516	34.875	55.60	1.83246	0.00366
L1_*Erik*	VUW	$10^{11}\Omega$	610.0	0.02	0.541	0.029	-0.455	0.010	77.0	31.7	0.754679	0.000005	7.0	327	22.040	73.40	0.87224	0.00174
L1_*Hank*	VUW	$10^{11}\Omega$	148.7	0.08	1.005	0.109	-0.676	0.024	320.3	80.5	0.754940	0.000020	25.9	190	46.062	154.90	0.86368	0.00173
L1_*Jean*	VUW	$10^{11}\Omega$	299.1	0.04	1.068	0.032	-0.972	0.011	75.6	33.3	0.796674	0.000006	7.3	339	38.376	73.86	1.51489	0.00303
L1_*Logan*	VUW	$10^{11}\Omega$	127.6	0.09	-0.743	0.060	0.842	0.017	124.8	53.7	0.936085	0.000009	9.9	185	28.743	22.63	3.75877	0.00752
L1_*Ororo*	VUW	$10^{11}\Omega$	1010.5	0.01	1.097	0.022	-0.953	0.009	123.3	27.8	0.869288	0.000005	5.8	517	37.735	45.07	2.45818	0.00492
L1_*Peter*	VUW	$10^{11}\Omega$	415.6	0.03	0.799	0.033	-0.687	0.010	98.7	35.0	0.792224	0.000005	6.9	327	33.902	67.36	1.46712	0.00293
L1_*Raven*	VUW	$10^{11}\Omega$	625.8	0.02	1.189	0.025	-1.064	0.009	98.2	29.4	0.775484	0.000005	6.5	515	64.186	160.06	1.16669	0.00233
L1_*Scott*	VUW	$10^{11}\Omega$	688.1	0.02	0.745	0.025	-0.629	0.010	100.7	29.0	0.827102	0.000005	6.1	515	41.756	61.88	1.97386	0.00395
Leach 2																		
L2_*Charles*	VUW	$10^{11}\Omega$	966.7	0.01	1.805	0.027	-1.664	0.012	100.9	29.8	0.736006	0.000005	6.6	516	24.059	115.77	0.60201	0.00120
L2_*Erik*	VUW	$10^{11}\Omega$	238.7	0.05	0.915	0.063	-0.820	0.015	74.5	52.7	0.705716	0.000008	11.0	191	17.897	434.06	0.11917	0.00024
L2_*Hank*	VUW	$10^{11}\Omega$	155.6	0.07	1.229	0.081	-1.093	0.015	120.6	71.3	0.700070	0.000009	13.1	116	1.426	165.52	0.02489	0.00005
L2_*Jean*	VUW	$10^{11}\Omega$	134.0	0.08	1.339	0.171	-1.277	0.018	89.4	148.1	0.701561	0.000015	21.8	158	1.916	93.03	0.05947	0.00012
L2_*Logan*	VUW	$10^{11}\Omega$	209.9	0.05	-0.132	0.061	0.379	0.015	259.9	53.7	0.702240	0.000007	9.7	220	3.114	199.91	0.04504	0.00009
L2_*Ororo*	VUW	$10^{11}\Omega$	3082.9	0.00	1.319	0.023	-1.209	0.011	81.9	27.5	0.731345	0.000005	6.6	516	22.309	119.54	0.54057	0.00108
L2_*Peter*	VUW	$10^{11}\Omega$	212.3	0.05	1.209	0.066	-1.039	0.020	141.2	56.2	0.702377	0.000008	11.9	144	29.479	1415.22	0.06017	0.00012
L2_*Raven*	VUW	$10^{11}\Omega$	286.5	0.04	1.263	0.082	-1.007	0.016	212.8	73.7	0.725027	0.000008	10.4	511	13.789	87.62	0.45562	0.00091
L2_*Scott*	VUW	$10^{11}\Omega$	1201.1	0.01	1.339	0.023	-1.172	0.012	140.5	27.3	0.711719	0.000005	6.8	516	21.007	304.84	0.19923	0.00040
Leach 3																		
L3_*Charles*	VUW	$10^{11}\Omega$	104.4	0.02	1.825	0.037	-1.633	0.014	149.5	35.1	0.704400	0.000006	7.9	289	0.952	30.68	0.08961	0.00018
L3_*Erik*	VUW	$10^{11}\Omega$	78.4	0.02	0.699	0.044	-0.597	0.015	96.0	40.2	0.699846	0.000007	9.5	153	0.102	23.07	0.01282	0.00003
L3_*Hank*	VUW	$10^{11}\Omega$	256.0	0.03	-0.986	0.032	1.027	0.014	66.7	32.1	0.699230	0.000005	7.6	441	0.107	75.06	0.00411	0.00001
L3_*Jean*	VUW	$10^{11}\Omega$	69.3	0.14	1.288	0.238	-1.147	0.029	102.0	210.6	0.700920	0.000018	26.4	148	0.189	20.33	0.02691	0.00005
L3_*Logan*	VUW	$10^{11}\Omega$	73.7	0.14	-0.374	0.151	0.494	0.019	113.8	140.7	0.701101	0.000011	16.4	147	0.149	21.65	0.01989	0.00004
L3_*Ororo*	VUW	$10^{11}\Omega$	61.6	0.02	1.082	0.035	-1.005	0.018	49.8	32.6	0.706083	0.000005	7.5	400	0.777	18.10	0.12402	0.00025
L3_*Peter*	VUW	$10^{11}\Omega$	85.8	0.07	1.377	0.136	-0.924	0.032	248.2	103.2	0.700116	0.000020	28.1	370	0.143	25.22	0.01636	0.00003
L3_*Raven*	VUW	$10^{11}\Omega$	79.3	0.03	0.971	0.046	-0.796	0.015	144.8	39.9	0.700493	0.000007	10.4	191	0.203	23.35	0.02508	0.00005
L3_*Scott*	VUW	$10^{11}\Omega$	101.0	0.03	0.830	0.097	-0.708	0.021	108.0	83.6	0.702521	0.000012	16.6	147	0.605	29.74	0.05880	0.00012
L3_*Jean*[6]	Bremen	$10^{11}\Omega$ on ^{88}Sr, $10^{13}\Omega$	69.3	0.14	1.464	0.061	-1.166	0.021	110.9	304.4	0.700914	0.000046	65.8	520	0.189	20.33	0.02691	0.00005
L3_*Logan*[6]	Bremen	$10^{11}\Omega$ on ^{88}Sr, $10^{13}\Omega$	73.7	0.14	-0.280	0.074	0.466	0.017	44.6	306.8	0.701081	0.000046	66.2	368	0.149	21.65	0.01989	0.00004

Table S4 (continued)

Sample number	Instrument	Amp. Config.	Total ng Sr in aliquot[1]	Blank contrib. %[2]	$\delta^{84/86}$Sr (‰)[3]	2 s.e.[5]	$\delta^{88/86}$Sr (‰)[3]	2 s.e.[5]	μ^{84}Sr (ppm)	2 s.e.[5]	^{87}Sr/^{86}Sr[3,4]	2 s.e.[5]	2 s.e. (ppm)	Cycles	Rb (ppm)[7]	Sr (ppm)[7]	^{87}Rb/^{86}Sr	2 s.e.
Leach 4																		
L4_*Charles*	Bremen	$10^{11}\Omega$ on ^{88}Sr, $10^{13}\Omega$	9.0	2.74	2.300	0.217	-0.242	0.073	1898.7	316.4	0.702108	0.000061	86.7	423	0.007	0.36	0.05313	0.00011
L4_*Erik*	Bremen	$10^{11}\Omega$ on ^{88}Sr, $10^{13}\Omega$	122.9	0.20	1.895	0.067	-1.611	0.027	84.1	305.2	0.698994	0.000046	66.2	338	0.015	7.88	0.00555	0.00001
L4_*Hank*	Bremen	$10^{11}\Omega$ on ^{88}Sr, $10^{13}\Omega$	12.9	1.91	-0.266	0.202	0.425	0.045	21.1	331.1	0.699180	0.000056	80.7	340	0.004	1.97	0.00581	0.00001
L4_*Jean*	Bremen	$10^{11}\Omega$ on ^{88}Sr, $10^{13}\Omega$	5.2	4.75	19.336	0.194	-0.661	0.061	18368.0	332.7	0.699349	0.000051	73.3	296	0.002	0.58	0.00845	0.00002
L4_*Logan*	Bremen	$10^{11}\Omega$ on ^{88}Sr, $10^{13}\Omega$	26.1	0.94	-0.729	0.072	1.119	0.028	245.2	306.1	0.699029	0.000046	66.3	302	0.009	12.98	0.00205	0.00000
L4_*Ororo*	Bremen	$10^{11}\Omega$ on ^{88}Sr, $10^{13}\Omega$	10.4	2.37	-0.626	0.116	1.167	0.066	416.7	309.1	0.701299	0.000048	68.0	514	0.004	0.27	0.04100	0.00008
L4_*Peter*	Bremen	$10^{11}\Omega$ on ^{88}Sr, $10^{13}\Omega$	12.9	1.90	1.734	0.235	0.547	0.169	2139.4	328.4	0.699480	0.000050	72.1	372	0.005	1.15	0.01146	0.00002
L4_*Raven*	Bremen	$10^{11}\Omega$ on ^{88}Sr, $10^{13}\Omega$	21.7	1.14	0.722	0.142	-0.460	0.053	95.1	319.3	0.699095	0.000049	69.5	185	0.002	1.74	0.00397	0.00001
L4_*Scott*	Bremen	$10^{11}\Omega$ on ^{88}Sr, $10^{13}\Omega$	8.9	2.77	0.762	0.257	-0.348	0.184	242.0	330.7	0.699372	0.000052	73.7	376	0.002	0.64	0.00913	0.00002
Leach 5																		
L5_*Charles*	Bremen	$10^{11}\Omega$ on ^{88}Sr, $10^{13}\Omega$	30.2	0.31	3.786	0.189	-1.820	0.103	1738.4	311.5	0.700716	0.000054	77.2	340	0.004	1.15	0.00936	0.00002
L5_*Erik*	Bremen	$10^{11}\Omega$ on ^{88}Sr, $10^{13}\Omega$	112.9	0.08	-0.847	0.055	1.089	0.024	119.0	304.1	0.700343	0.000046	65.3	448	0.011	16.58	0.00199	0.00000
L5_*Hank*	Bremen	$10^{11}\Omega$ on ^{88}Sr, $10^{13}\Omega$	0.4	24.82	81.405	2.495	0.251	0.819	80654.6	1806.8	0.704163	0.000242	343.6	104	0.003	2.11	0.00406	0.00001
L5_*Jean*	Bremen	$10^{11}\Omega$ on ^{88}Sr, $10^{13}\Omega$	1.3	7.07	3.644	0.995	-1.955	0.362	1491.9	837.7	0.699861	0.000116	165.7	157	0.006	1.80	0.00902	0.00002
L5_*Logan e.c.*																		
L5_*Ororo*	Bremen	$10^{11}\Omega$ on ^{88}Sr, $10^{13}\Omega$	11.2	0.82	13.779	0.164	-1.958	0.125	11598.9	304.8	0.701080	0.000048	68.7	370	0.001	0.31	0.01122	0.00002
L5_*Peter*	Bremen	$10^{11}\Omega$ on ^{88}Sr, $10^{13}\Omega$	1.4	6.77	4.259	0.686	0.936	0.388	5224.9	522.4	0.701344	0.000088	126.1	323	0.027	2.41	0.03198	0.00006
L5_*Raven*	Bremen	$10^{11}\Omega$ on ^{88}Sr, $10^{13}\Omega$	50.2	0.18	1.296	0.748	-0.792	0.170	320.4	448.6	0.699209	0.000154	220.0	110	0.015	3.49	0.01267	0.00003
L5_*Scott*	Bremen	$10^{11}\Omega$ on ^{88}Sr, $10^{13}\Omega$	58.2	0.16	0.755	0.076	0.237	0.044	854.5	304.6	0.706701	0.000046	65.3	372	0.025	5.51	0.01329	0.00003
Bulk CAI																		
Charles	VUW	$10^{11}\Omega$, $10^{13}\Omega$ on ^{84}Sr	132.5	0.05	-	-	-	-	181.2	52.2	0.763824	0.000009	11.9	119	8.119	23.48	1.00583	0.01182
Erik	VUW	$10^{11}\Omega$, $10^{13}\Omega$ on ^{84}Sr	110.1	0.06	-	-	-	-	153.8	53.3	0.720482	0.000008	10.8	188	3.574	30.67	0.33748	0.00391
Hank	VUW	$10^{11}\Omega$, $10^{13}\Omega$ on ^{84}Sr	59.5	0.11	-	-	-	-	158.6	70.7	0.710660	0.000010	14.6	115	3.105	54.43	0.16507	0.00187
Jean	VUW	$10^{11}\Omega$, $10^{13}\Omega$ on ^{84}Sr	68.6	0.10	-	-	-	-	230.0	72.6	0.757596	0.000010	13.7	107	7.885	25.50	0.89888	0.01052
Logan	VUW	$10^{11}\Omega$, $10^{13}\Omega$ on ^{84}Sr	85.7	0.08	-	-	-	-	284.8	96.9	0.771961	0.000016	20.5	98	13.190	34.10	1.12586	0.01299
Ororo	VUW	$10^{11}\Omega$, $10^{13}\Omega$ on ^{84}Sr	213.6	0.03	-	-	-	-	141.2	56.5	0.757357	0.000008	10.5	165	8.540	28.51	0.87069	0.00972
Peter	VUW	$10^{11}\Omega$, $10^{13}\Omega$ on ^{84}Sr	62.6	0.11	-	-	-	-	171.4	82.0	0.752229	0.000011	14.9	77	8.393	29.59	0.82402	0.00911
Raven	VUW	$10^{11}\Omega$, $10^{13}\Omega$ on ^{84}Sr	177.9	0.04	-	-	-	-	141.0	52.1	0.743839	0.000007	10.0	282	6.368	26.87	0.68803	0.00788
Scott	VUW	$10^{11}\Omega$, $10^{13}\Omega$ on ^{84}Sr	313.6	0.02	-	-	-	-	140.6	51.5	0.745719	0.000007	9.4	266	10.019	43.86	0.66321	0.00813

[1]Total Sr in aliquot prior to further aliquotting for isotope work

[2]Procedural blank contribution to each of the 50% aliquots taken for double spike and 'natural' analysis, total blank contribution for bulk analyses

[3]Isotope ratios corrected for blank contribution

[4]Normalized to ^{87}Sr/^{86}Sr = 0.710250 for NBS987 for comparison with other published work

[5]2s.e. uncertainties represent within-run uncertainties quadratically added to external reproducibility of the standards for the relevant instrument

[6]Samples measured on both the VUW and Bremen instruments

[7]Elemental concentrations in material digested during each leach step

e.c. = entirely consumed

- = No double spike measurements made

Table S5. Calculated slopes (± 95% CI and MSWD) for best fit lines in natural log three-isotope space for two NBS987 standards and three 'synthetic CAI' mixtures processed through the column separation procedure. Expected values are slopes calculated assuming exponential law fractionation (*14*).

	$\ln^{84}sr/^{87}Sr$ vs. $\ln^{88}Sr/^{87}Sr$	2σ	MSWD	$\ln^{86}sr/^{87}Sr$ vs. $\ln^{88}Sr/^{87}Sr$	2σ	MSWD	$\ln^{86}sr/^{87}Sr$ vs. $\ln^{84}Sr/^{87}Sr$	2s	MSWD
NBS987_1	-0.318	0.005	4.3	-0.982	0.01	2.7	3.072	0.042	2.9
NBS987_2	-0.3251	0.003	3.3	-0.9875	0.0061	1.8	3.041	0.021	1.8
CAIsoln_1	-0.3246	0.0023	3.5	-0.9847	0.005	2.2	3.032	0.019	2.5
CAIsoln_2	-0.3221	0.0065	7.5	-0.97	0.013	4.7	3.026	0.058	6.7
CAIsoln_3	-0.321	0.018	6.5	-0.992	0.034	2.9	3.09	0.16	6
expected	*-0.3251*			*-0.9857*			*3.0319*		

Table S6. Strontium content and isotopic composition for the four dental tools used for CAI extraction, along with four 1 ng loads of NBS987 measured during the same session (using the VUW TIMS instrument).

Tool name	Material[1]	Sample weight (mg)	Sr (ppb)	$^{84}Sr/^{86}Sr$	2 s.e.	2 s.e. ppm	$\mu^{84}Sr$	$^{87}Sr/^{86}Sr$	2 s.e.	2 s.e. ppm
DT-1	SS	73.88	71.3	0.056509	0.000031	550	198	0.70835	0.000054	77
DT-2	SS	100.77	215.6	0.056465	0.000066	1168	-591	0.70907	0.000085	119
DT-3	NiCoMo	110.22 (59.23)[2]	14.8	0.056494	0.000024	421	-66	0.71001	0.000044	62
DT-4	SS	109.63	16.6	0.056423	0.000030	534	-1334	0.70934	0.000068	96
NBS987 1ng_1				0.056508	0.000023	404	169	0.71027	0.000042	59
NBS987 1ng_2				0.056482	0.000023	404	-279	0.71022	0.000045	63
NBS987 1ng_3				0.056507	0.000021	369	160	0.71027	0.000039	55
NBS987 1ng_4				0.056495	0.000020	352	-51	0.71024	0.000040	57
Average				0.056498				0.71025		
2 s.d.				0.000024				0.000052		
2 s.d. ppm				424				73		

REFERENCES AND NOTES

1. Y. Amelin, A. Kaltenbach, T. Iizuka, C. H. Stirling, T. R. Ireland, M. Petaev, S. B. Jacobsen, U–Pb chronology of the Solar System's oldest solids with variable $^{238}U/^{235}U$. *Earth Planet. Sci. Lett.* **300**, 343–350 (2010).

2. J. N. Connelly, M. Bizzarro, A. N. Krot, Å. Nordlund, D. Wielandt, M. A. Ivanova, The absolute chronology and thermal processing of solids in the solar protoplanetary disk. *Science* **338**, 651–655 (2012).

3. P. J. Patchett. Sr isotopic fractionation in Ca–Al inclusions from the Allende meteorite. *Nature* **283**, 438–441 (1980).

4. B. L. A. Charlier, F. L. H. Tissot, N. Dauphas, C. J. N. Wilson, Nucleosynthetic, radiogenic and stable strontium isotopic variations in fine- and coarse-grained refractory inclusions from Allende. *Geochim. Cosmochim. Acta* **265**, 413–430 (2019).

5. D. A. Papanastassiou, G. J. Wasserburg, Strontium isotopic anomalies in the Allende meteorite. *Geophys. Res. Lett.* **5,** 595–598 (1978).

6. C. Paton, M. Schiller, M. Bizzarro, Identification of an ^{84}Sr-depleted carrier in primitive meteorites and implications for thermal processing in the solar protoplanetary disk. *Astrophys. J. Lett.* **763**, L40 (2013).

7. T. Yokoyama, Y. Fukami, W. Okui, N. Ito, H. Yamazaki, Nucleosynthetic strontium isotope anomalies in carbonaceous chondrites. *Earth Planet. Sci. Lett.* **416**, 46–55 (2015).

8. B. L. A. Charlier, I. J. Parkinson, K. W. Burton, M. M. Grady, C. J. N. Wilson, E. G. C. Smith, Stable strontium isotopic heterogeneity in the solar system from double-spike data. *Geochem. Perspect. Lett.* **4**, 35–40 (2017).

9. K. Myojo, T. Yokoyama, S. Okabayashi, S. Wakaki, N. Sugiura, H. Iwamori, The origin and evolution of nucleosynthetic Sr isotope variability in calcium and aluminium-rich refractory inclusions. *Astrophys. J.* **853**, 48 (2018).

10. C. Burkhardt, N. Dauphas, U. Hans, B. Bourdon, T. Kleine, Elemental and isotopic variability in solar system materials by mixing and processing of primordial disk reservoirs. *Geochim. Cosmochim. Acta* **261**, 145–170 (2019).

11. D. A. Papanastassiou, G. J. Wasserburg, Initial strontium isotopic abundances and the resolution of small time differences in the formation of planetary objects. *Earth Planet. Sci. Lett.* **5**, 361–376 (1969).

12. A. N. Halliday, D. Porcelli, In search of lost planets – the paleocosmochemistry of the inner solar system. *Earth Planet. Sci. Lett.* **192**, 545–559 (2001).

13. F. Moynier, J. M. D. Day, W. Okui, T. Yokoyama, A. Bouvier, R. J. Walker, F. A. Podosek, Planetary-scale strontium isotopic heterogeneity and the age of volatile depletion of early solar system materials. *Astrophys. J.* **758**, 45 (2012).

14. E. D. Young, A. Galy, H. Nagahara, Kinetic and equilibrium mass-dependent isotope fractionation laws in nature and their geochemical and cosmochemical significance. *Geochim. Cosmochim. Acta* **66**, 1095–1104 (2002).

15. F. Moynier, A. Agranier, D. C. Hezel, A. Bouvier, Sr stable isotope composition of Earth, the Moon, Mars, Vesta and meteorites. *Earth Planet. Sci. Lett.* **300**, 359–366 (2010).

16. B. L. A. Charlier, G. M. Nowell, I. J. Parkinson, S. P. Kelley, D. G. Pearson, K. W. Burton, High temperature strontium stable isotope behaviour in the early solar system and planetary bodies. *Earth Planet. Sci. Lett.* **329-330**, 31–40 (2012).

17. U. Hans, T. Kleine, B. Bourdon, Rb–Sr chronology of volatile depletion in differentiated protoplanets: BABI, ADOR and ALL revisited. *Earth Planet. Sci. Lett.* **374**, 204–214 (2013).

18. G. A. Brennecka, L. E. Borg, M. Wadhwa, Evidence for supernova injection into the solar nebula and the decoupling of *r*-process nucleosynthesis. *Proc. Natl. Acad. Sci. U.S.A.* **110**, 17241–17246 (2013).

19. Q. R. Shollenberger, L. E. Borg, J. Render, S. Ebert, A. Bischoff, S. S. Russell, G. A. Brennecka, Isotopic coherence of refractory inclusions from CV and CK meteorites: Evidence from multiple isotope systems. *Geochim. Cosmochim. Acta* **228**, 62–80 (2018).

20. K. Lodders, Solar system abundances and condensation temperatures of the elements. *Astrophys. J.* **591**, 1220–1247 (2003).

21. F. A. Podosek, E. K. Zinner, G. J. MacPherson, L. L. Lundberg, J. C. Brannon, A. J. Fahey, Correlated study of initial $^{87}Sr/^{86}Sr$ and Al-Mg isotopic systematics and petrologic properties in a suite of refractory inclusions from the Allende meteorite. *Geochim. Cosmochim. Acta* **55**, 1083–1110 (1991).

22. D. A. Papanastassiou, Initial $^{87}Sr/^{86}Sr$ chronology; a journey through 4.5 decades, in *Proceedings of the 46th Lunar Planetary Science Conference,* (2015), 2243.

23. D. A. Papanastassiou, J. H. Chen, Initial $^{87}Sr/^{86}Sr$ chronology in the solar system, in *Proceedings of the 47th Lunar Planetary Science Conference*, (2016), 2650.

24. C. M. Gray, D. A. Papanastassiou, G. J. Wasserburg, The identification of early condensates from the solar nebula. *Icarus* **20**, 213–239 (1973).

25. L. Grossman, R. M. Fruland, D. S. McKay, Scanning electron microscopy of a pink inclusion from the Allende meteorite. *Geophys. Res. Lett.* **2**, 37–40 (1975).

26. L. Grossman, Condensation in the primitive solar nebula. *Geochim. Cosmochim. Acta* **36**, 597–619 (1972).

27. S. Yoneda, L. Grossman, Condensation of $CaO–MgO–Al_2O_3–SiO_2$ liquids from cosmic gases. *Geochim. Cosmochim. Acta* **59**, 3413–3444 (1995).

28. D. S. Ebel, Condensation of rocky material in astrophysical environments, in *Meteorites and the Early Solar System II*, D. S. Lauretta, H. Y. McSween Jr., Eds. (University of Arizona Press, 2006), pp. 253–277.

29. J. Y. Hu, N. Dauphas, F. L. H. Tissot, R. Yokochi, T. J. Ireland, Z. Zhang, A. M. Davis, F. J. Ciesla, L. Grossman, B. L. A. Charlier, M. Roskosz, E. E. Alp, M. Y. Hu, J. Zhao, Heating events in the nascent solar system recorded by rare earth element isotopic fractionation in refractory inclusions. *Sci. Adv.* **7**, eabc2962 (2021).

30. J. M. Koornneef, C. Bouman, J. B. Schwieters, G. R. Davies, Measurement of small ion beams by thermal ionisation mass spectrometry using new 10^{13} Ohm resistors. *Anal. Chim. Acta* **819**, 49–55 (2014).

31. G. J. MacPherson, C. Defouilloy, N. T. Kita, High-precision Al–Mg isotopic systematics in USNM 3898–The benchmark "ALL" for initial $^{87}Sr/^{86}Sr$ in the earliest Solar System. *Earth Planet. Sci. Lett.* **491**, 238–243 (2018).

32. Y. Amelin, C. D. Williams, M. Wadhwa, U-Th-Pb and Rb-Sr systematics of Allende FUN CAI CMS-1, in *Proceedings of the 46th Lunar Planetary Science Conference*, (2015), 2355.

33. G. R. Huss, The survival of presolar grains in solar system bodies. *AIP Conf. Proc.* **402**, 721–748 (1997).

34. G. R. Huss, R. S. Lewis, Presolar diamond, SiC, and graphite in primitive chondrites: Abundances as a function of meteorite class and petrologic type. *Geochim. Cosmochim. Acta* **59**, 115–160 (1995).

35. E. K. Zinner, Presolar grains, in *Treatise on Geochemistry, Vol. 1, Meteorites, Comets, and Planets*, H. D. Holland, K. K. Turekian, A. M. Davis, Eds. (Elsevier, 2003), pp. 1–33.

36. O. Pravdivtseva, F. L. H. Tissot, N. Dauphas, S. Amari, Evidence of presolar SiC in the Allende Curious Marie calcium-aluminium-rich inclusion. *Nat. Astron.* **4**, 617–624 (2020).

37. G. K. Nicolussi, M. J. Pellin, R. S. Lewis, A. M. Davis, R. N. Clayton, S. Amari, Strontium isotopic composition in individual circumstellar silicon carbide grains: A record of *s*-process nucleosynthesis. *Phys. Rev. Lett.* **81**, 3583–3586 (1998).

38. T. Stephan, R. Trappitsch, A. M. Davis, M. J. Pellin, D. Rost, M. R. Savina, M. Jadhav, C. H. Kelly, F. Gyngard, P. Hoppe, N. Dauphas, Strontium and barium isotopes in presolar silicon carbide grains measured with CHILI—Two types of X grains. *Geochim. Cosmochim. Acta* **221**, 109–126 (2018).

39. T. Stephan, R. Trappitsch, P. Hoppe, A. M. Davis, M. J. Pellin, O. S. Pardo, Molybdenum isotopes in presolar silicon carbide grains: Details of *s*-process nucleosynthesis in parent stars and implications for *r*-and *p*-processes. *Astrophys. J.* **877**, 101 (2019).

40. T. Rauscher, N. Dauphas, I. Dillmann, C. Fröhlich, Z. Fülöp, G. Gyürky, Constraining the astrophysical origin of the *p*-nuclei through nuclear physics and meteoritic data. *Rep. Prog. Phys.* **76**, 066201 (2013).

41. T. Rauscher, A. Heger, R. D. Hoffman, S. E. Woosley, Nucleosynthesis in massive stars with improved nuclear and stellar physics. *Astrophys. J.* **576**, 323–348 (2002).

42. C. Travaglio, F. K. Röpke, R. Gallino, W. Hillebrandt, Type Ia supernovae as sites of the *p*-process: Two-dimensional models coupled to nucleosynthesis. *Astrophys. J.* **739**, 93 (2011).

43. G. R. Huss, R. S. Lewis, Noble gases in presolar diamonds I: Three distinct components and their implications for diamond origins. *Meteoritics* **29**, 791–810 (1994).

44. G. R. Huss, A. P. Meshik, J. B. Smith, C. M. Hohenberg, Presolar diamond, silicon carbide, and graphite in carbonaceous chondrites: Implications for thermal processing in the solar nebula. *Geochim. Cosmochim. Acta* **67**, 4823–4848 (2003).

45. N. Dauphas, E. A. Schauble, Mass fractionation laws, mass-independent effects, and isotopic anomalies. *Annu. Rev. Earth Planet. Sci.* **44**, 709–783 (2016).

46. P. H. Warren, Stable-isotopic anomalies and the accretionary assemblage of the Earth and Mars: A subordinate role for carbonaceous chondrites. *Earth Planet. Sci. Lett.* **311**, 93–100 (2011).

47. S. Gerber, C. Burkhardt, G. Budde, K. Metzler, T. Kleine, Mixing and transport of dust in the early solar nebula as inferred from titanium isotope variations among chondrules. *Astrophys. J. Lett.* **841**, L17 (2017).

48. J. A. Nanne, F. Nimmo, J. N. Cuzzi, T. Kleine, Origin of the non-carbonaceous–carbonaceous meteorite dichotomy. *Earth Planet. Sci. Lett.* **511**, 44–54 (2019).

49. G. Budde, C. Burkhardt, T. Kleine, Molybdenum isotopic evidence for the late accretion of outer Solar System material to Earth. *Nat. Astron.* **3**, 736–741 (2019).

50. F. C. Pignatale, S. Charnoz, M. Chaussidon, E. Jacquet, Making the planetary material diversity during the early assembling of the solar system. *Astrophys. J. Lett.* **867**, L23 (2018).

51. T. Kleine, U. Hans, A. J. Irving, B. Bourdon, Chronology of the angrite parent body and implications for core formation in protoplanets. *Geochim. Cosmochim. Acta* **84**, 186–203 (2012).

52. Y. Di, Y. Amelin, Heterogeneous nucleosynthetic 84Sr anomalies within and among CAIs, in proceedings of the 2020 Goldschmidt Conference (2020), 21 to 26 June, https://doi.org/10.46427/gold2020.570.

53. G. W. Lugmair, S. J. G. Galer, Age and isotopic relationships among the angrites Lewis Cliff-86010 and Angra dos Reis. *Geochim. Cosmochim. Acta* **56**, 1673–1694 (1992).

54. F. L. H. Tissot, N. Dauphas, L. Grossman, Origin of uranium isotope variations in early solar nebula condensates. *Sci. Adv.* **2**, e1501400 (2016).

55. L. Grossman, R. Ganapathy, Trace elements in the Allende meteorite—II. Fine-grained. Ca-rich inclusions. *Geochim. Cosmochim. Acta* **40**, 967–977 (1976).

56. A. N. Krot, G. J. MacPherson, A. A. Ulyanov, M. I. Petaev, Fine-grained, spinel-rich inclusions from the reduced CV chondrites Efremovka and Leoville: I. Mineralogy, petrology, and bulk chemistry. *Meteor. Planet. Sci.* **39**, 1517–1553 (2004).

57. A. Hashimoto, L. Grossman, SEM-petrography of Allende fine-grained inclusions, in *Proceedings of the 16th Lunar Planetary Science Conference* (1985), Houston, Texas, 11 to 15 March 1985, pp. 323–324.

58. A. Trinquier, J.-L. Birck, C. J. Allegre, Widespread ^{54}Cr heterogeneity in the inner solar system. *Astrophys. J.* **655**, 1179–1185 (2007).

59. K. J. R. Rosman, P. D. P. Taylor, Isotopic compositions of the elements 1997 (Technical Report). *Pure Appl. Chem.* **70**, 217–235 (1998).

60. B. L. A. Charlier, C. Ginibre, D. Morgan, G. M. Nowell, D. G. Pearson, J. P. Davidson, C. J. Ottley, Methods for the microsampling and high-precision analysis of strontium and rubidium isotopes at single crystal scale for petrological and geochronological applications. *Chem. Geol.* **232**, 114–133 (2006).

61. K. R. Ludwig, Isoplot/Ex Version 2.49: A geochronological toolkit for Microsoft Excel (Berkeley Chronology Center, Berkeley, CA, 2002).

62. E. Rotenberg, D. W. Davis, Y. Amelin, S. Ghosh, B. A. Bergquist, Determination of the decay-constant of ^{87}Rb by laboratory accumulation of ^{87}Sr. *Geochim. Cosmochim. Acta* **85**, 41–57 (2012).

63. N. Dauphas, A. Pourmand, Thulium anomalies and rare earth element patterns in meteorites and Earth: Nebular fractionation and the nugget effect. *Geochim. Cosmochim. Acta* **163**, 234–261 (2015).

64. R. T. M. Marquez, B. L. A. Charlier, F. L. H. Tissot, Search for the carriers of anomalous nucleosynthetic signatures in early solar system condensates, in *Proceedings of the 52nd Lunar Planetary Science Conference* (2021), 15 to 19 March 2021, id. 2635.